Smart Structures and Systems, *Vol. 14, No. 6 (2014) 1221-1245*
DOI: http://dx.doi.org/10.12989/sss.2014.14.6.1221

Establishing a stability switch criterion for effective implementation of real-time hybrid simulation

Amin Maghareh[*1], Shirley J. Dyke[2], Arun Prakash[1] and Jeffrey F. Rhoads[2]

[1]*School of Civil Engineering, Purdue University, West Lafayette, IN 47906, USA*
[2]*School of Mechanical Engineering, Purdue University, West Lafayette, IN 47906, USA*

(Received March 9, 2014, Revised August 25, 2014, Accepted August 30, 2014)

Abstract. Real-time hybrid simulation (RTHS) is a promising cyber-physical technique used in the experimental evaluation of civil infrastructure systems subject to dynamic loading. In RTHS, the response of a structural system is simulated by partitioning it into physical and numerical substructures, and coupling at the interface is achieved by enforcing equilibrium and compatibility in real-time. The choice of partitioning parameters will influence the overall success of the experiment. In addition, due to the dynamics of the transfer system, communication and computation delays, the feedback force signals are dependent on the system state subject to delay. Thus, the transfer system dynamics must be accommodated by appropriate actuator controllers. In light of this, guidelines should be established to facilitate successful RTHS and clearly specify: (i) the minimum requirements of the transfer system control, (ii) the minimum required sampling frequency, and (iii) the most effective ways to stabilize an unstable simulation due to the limitations of the available transfer system. The objective of this paper is to establish a stability switch criterion due to systematic experimental errors. The RTHS stability switch criterion will provide a basis for the partitioning and design of successful RTHS.

Keywords: real-time hybrid simulation; RTHS; RTHS stability criterion; stability switch criterion

1. Introduction

As civil structures evolve to meet the needs of future generations, there is an increasing demand to demonstrate the effectiveness of performance-based design, utilize new materials capable of reducing earthquake impact, and improve retrofitting strategies (Dyke *et al*. 2010). These challenges justify the need for more comprehensive experimental capabilities in evaluating structural response and performance in a suitable and cost-effective manner. Currently, three main experimental methods exist to evaluate structural behavior in the presence of dynamic loads: (1) shake table testing, (2) quasi-static testing, and (3) hybrid simulation (Mosqueda *et al*. 2005).

Shake table testing enables researchers to produce realistic test conditions and evaluate critical issues such as collapse mechanisms, component failures, acceleration amplifications, residual displacements and post-earthquake capacities independently (Schellenberg and Mahin 2006). In the seismic evaluation of civil structures using shake table testing, a researcher needs to know the required actuator's peak velocity (directly related to the oil flow rate provided by the pumping

*Corresponding author, Ph.D. Student, E-mail: amaghare@purdue.edu

http://www.techno-press.org/?journal=sss&subpage=8 ISSN: 1738-1584 (Print), 1738-1991 (Online)

system and servo-valve), the rated capacity of the actuator, the maximum stroke, and the actuator's frequency bandwidth (Dihoru and Bonzi 2010). Considering these well-defined parameters, there is usually no stability concern, and the results are reliable. However, very few shake tables in the world are capable of testing full-scale large civil structures; thus, shake table testing is often limited to prototypes, limited in payload, and prohibitively expensive (Shing *et al.* 1996).

Quasi-static testing is another experimental technique in which the structure (or component) under investigation is subject to a predefined displacement history at a slow rate. Usually, this technique is applied to study the hysteretic and cyclic behavior of structural components subject to seismic loading (Carrion and Spencer 2007). While quasi-static testing can be implemented on large civil structures, it has two major drawbacks: it requires a predefined displacement history (Shing and Mahin 1984); and it does not preserve rate-dependence while evaluating the dynamic performance of structures.

Hybrid simulation (HS) is a cost-effective experimental technique used to evaluate the dynamic performance of large civil structures. In hybrid simulation, the structure under investigation (i.e., the reference structure) is partitioned into two substructures: (i) a physical (or experimental) substructure, which usually includes the structure's more complex components; and (ii) a numerical (or analytical) substructure, which usually includes well-understood components. Coupling between the two substructures is achieved by enforcing equilibrium and compatibility at the interface (Chen *et al*. 2012).

Real-time hybrid simulation is a powerful experimental technique used to evaluate the performance of civil systems when rate-dependence plays a role. In RTHS, the interface interaction between the substructures is enforced by a transfer system which includes servo-hydraulic actuator(s) and/or a shake table (Wallace *et al*. 2005). The transfer system should be designed and controlled to ensure that all the interface boundary conditions are satisfied in real-time (Wagg and Stoten 2001). Fig. 1 depicts a typical real-time hybrid simulation of a four-story structure where hydraulic actuators are used to satisfy the interface boundary conditions.

A number of researchers have used this cyber-physical technique to successfully evaluate the seismic performance of structures, examine different structural control algorithms and techniques, and develop guidelines for the implementation of damping systems in civil infrastructures. Many examples of this can be found in the project repository of the George E. Brown Network for Earthquake Engineering Simulation (http://www.nees.org/). To name a few, Mosqueda *et al*. increased the complexity of the structural models employed in RTHS using geographically-distributed substructures and investigated the procedures for evaluating the reliability of the results in real-time (Gilberto *et al*. 2007a, Gilberto *et al.* 2007b, Mosqueda *et al*. 2005). Christenson *et al*. implemented RTHS to evaluate the relative efficacy of smart damping control devices (Christenson *et al*. 2008) and Shao *et al*. conducted force-based substructuring in RTHS (Shao *et al*. 2011). Gao and Castaneda implemented and validated some small-scale frame structural configurations equipped with damper devices to develop a robust framework for RTHS (Gao 2012, Castaneda *et al.* 2012). Later, some researchers developed and validated performance-based design guidelines for the implementation of advanced damping systems in civil infrastructure using RTHS (Friedman *et al*. 2010, Jiang and Christenson 2011, Phillips and Spencer 2013).

RTHS is a complex cyber-physical technique, and progress in this cutting-edge research area necessitates expertise from highly-interdisciplinary research teams. Clearly, the test set-up will affect the stability and performance of the system. Stability and performance of RTHS are mainly functions of four entities: (1) the overall dynamics of the reference structure, (2) the fidelity of the

numerical substructure, (3) how the reference structure is partitioned into the numerical and physical substructures, and (4) how well the interface boundary conditions are achieved by the transfer system. Several researchers have investigated the impact of these entities on stability and reliability of simulations (Darby *et al*. 2002, Gilberto *et al*. 2007a, Mosqueda *et al*. 2007, Chen and Ricles 2009, Gao 2012, Chen *et al*. 2013, Maghareh *et al.* 2012). In addition, Maghareh *et al*. have proposed two pre-experiment metrics for RTHS, predictive stability indicator (PSI) and predictive performance indicator (PPI) (Maghareh and Dyke 2013, Maghareh *et al*. 2013).

Transfer system control plays a critical role in RTHS. Effective transfer system control leads to an accurate tracking of the desired boundary condition between the substructures. Because servo-hydraulic actuators (or shake tables) are dynamic systems, time lags may be present due to the physical limitations/dynamics of the transfer system. Time lags, undesirable dynamics of the transfer system, and measurement noise in the feedback force signal(s) can destabilize the simulation (Horiuchi *et al*. 1999, Gao 2012) and/or excite spurious lightly-damped modes of the system (Maghareh *et al*. 2013). To realize the desired boundary conditions between the substructures in real-time, Horiuchi *et al*. proposed the polynomial extrapolation delay compensation method (Horiuchi *et al*. 1996). Later, other researchers developed more sophisticated controllers/compensators, see for example (Chen *et al*. 2012, Gao 2012, Phillips and Spencer 2013, Ou *et al*. 2013). With recently conducted research on transfer system control/compensation, undesirable dynamics of the transfer system can be diminished, but cannot be completely eliminated, even with the most sophisticated techniques (Chen *et al.* 2013).

Errors in RTHS stem from three different sources: model idealization, numerical integration, and experimental errors. Modeling error arises from any discrepancies between the response of the actual (or real) portion modeled as a numerical substructure and the response acquired from its model. In addition, in RTHS, explicit or implicit integration schemes are utilized to solve the idealized numerical substructure. Depending upon which integration scheme is adopted, stability and accuracy issues may be limiting factors (Mosqueda *et al*. 2005). Finally, in RTHS, there are a number of experimental sources of error which can be divided into two subcategories: epistemic and aleatoric errors. Sources of epistemic errors are systematic, such as transfer system dynamics, computational delays, communication delays, and sensor miscalibration. However, sources of aleatoric errors are random, such as measurement noise and random truncations in the analog-to-digital (AD) conversions of signals.

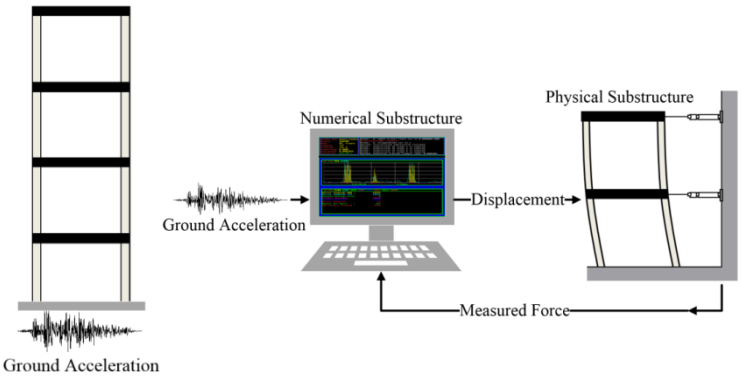

Fig. 1 A typical real-time hybrid simulation of a four-story structure

In the current approach, prior to conducting an RTHS, a specific sampling frequency and a transfer system controller/compensator are adopted. To choose a suitable sampling frequency, usually equal to or larger than 1024 Hz, the user determines the minimum time required to solve the discretized governing equation of the numerical substructure and the largest natural frequency of the numerical model assuming linear dynamics. A control/compensation technique is then adopted and its parameters are tuned accordingly. Finally, to avoid instability, the stability of the whole system is examined using a simulation of the RTHS which includes the numerical substructure, a model of the transfer system, and a model of the physical substructure. While this approach is conceptually attractive, to make RTHS more accessible to structural engineers, guidelines need to be established to clearly specify: (a) the minimum requirements of the transfer system control, (b) the minimum required sampling frequency, and (c) the most effective ways to stabilize an unstable RTHS due to the limitations of the available transfer system.

To conduct a successful RTHS, global stability and performance are the major issues. In this study, we focus on the stability aspect of RTHS systems and the issue of performance is being addressed in a related study (Maghareh *et al*. 2013). The objective of this paper is twofold: (i) to establish an RTHS stability switch criterion that can be used as a predictive stability indicator, and (ii) to develop an RTHS design guideline associated with the minimum requirements for the transfer system control and sampling frequency. Herein, RTHS is modeled by a set of delay differential equations (DDE's). The main parameters investigated in this study are: (1) the structural characteristics of the reference structure (e.g., natural frequency, damping ratio, and structural nonlinearity), (2) the partitioning parameters, and (3) systematic experimental errors in RTHS, such as transfer system dynamics, computational/communication delays. Finally, an illustrative experiment is conducted to delineate the RTHS stability switch criterion, demonstrate an application of the RTHS design guidelines, and show the feasible/infeasible regions associated with the transfer system's performance. The corresponding data is provided in (Maghareh *et al*. 2014).

2. Modeling of RTHS systems

The governing equation of a general reference structure can be expressed as

$$[\mathrm{M}]\ddot{\mathrm{X}}(\mathrm{t}) + [\mathrm{C}]\dot{\mathrm{X}}(\mathrm{t}) + \mathrm{R}(\mathrm{X}) = -[\mathrm{M}]\Gamma\ddot{x}_g \tag{1}$$

where $[\mathrm{M}]$, $[\mathrm{C}]$, $\mathrm{R}(\mathrm{X})$, Γ, $\mathrm{X}(\mathrm{t})$, and $\ddot{x}_g$ are the structure's mass matrix, damping matrix, restoring force vector, influence vector, displacement vector, and ground acceleration, respectively. In RTHS, the reference structure is partitioned into numerical and physical substructures

$$\{[\mathrm{M}], [\mathrm{C}], \mathrm{R}(\mathrm{X})\} = \left\{\left[\mathrm{M}_p\right], \left[\mathrm{C}_p\right], \mathrm{R}_p(\mathrm{X})\right\} + \{[\mathrm{M}_n], [\mathrm{C}_n], \mathrm{R}_n(\mathrm{X})\} \tag{2}$$

where p and n indices refer to the physical and numerical substructures. The governing equation of the numerical substructure can be expressed as

$$[\mathrm{M}_n]\ddot{\mathrm{X}}(\mathrm{t}) + [\mathrm{C}_n]\dot{\mathrm{X}}(\mathrm{t}) + \mathrm{R}_n(\mathrm{X}) = -[\mathrm{M}]\Gamma\ddot{x}_g - F_{fb}(t) \tag{3}$$

where $F_{fb}(t)$ is the interaction force vector measured in the physical substructure and used as a

feedback signal into the numerical substructure. In an ideal case, $F_{fb}(t)$ can be defined as

$$F_{fb}(t) = [\mathrm{M}_p]\ddot{\mathrm{X}}(\mathrm{t}) + [\mathrm{C}_p]\dot{\mathrm{X}}(\mathrm{t}) + \mathrm{R}_p(\mathrm{X}) \quad (4)$$

Combining equations Eqs. (3) and (4) yields the governing equation of the reference structure in Eq. (1). However, the ideal case requires perfect control over the transfer system, no measurements noise, no time delay, and that all of the boundary conditions are satisfied perfectly. Due to transfer system control limitations and the time delay in the feedback signal, the governing equation of an RTHS system becomes

$$[\mathrm{M}_n]\ddot{\mathrm{X}}(\mathrm{t}) + [\mathrm{C}_n]\dot{\mathrm{X}}(\mathrm{t}) + \mathrm{R}_n(\mathrm{X}) = -[\mathrm{M}]\Gamma\ddot{x}_g - T\{\sum a_i F_{fb}(t-\tau_i), \sum b_i \dot{F}_{fb}(t-\tau_i), \ldots\} \quad (5)$$

where $T\{\ldots\}$ is an operator representing the effect of the transfer system dynamics and $F_{fb}(t-\tau)$ indicates time delay in the feedback force signal. In RTHS, time lags and time delays can be classified into three major categories: (1) communication delays, (2) computational delays, and (3) transfer system dynamics. Fig. 2 demonstrates a general, distributed RTHS architecture with multiple physical substructures and a numerical substructure. In addition, the presence of the communication and computational delays and transfer system dynamics are shown.

2.1 Communication delay

To implement RTHS, there is a continuous exchange of information between the cyber and physical components. In RTHS, communication delays vary from almost negligible for an RTHS using a single processor (no network) to more than a hundred milliseconds for geographically-distributed testing. Geographically-distributed RTHS presents a challenge in which the required communication over the Internet results in random delays (Mosqueda *et al.* 2005). Thus, communication delays become significant source of instability when conducting geographically-distributed RTHS (Carrion and Spencer 2007).

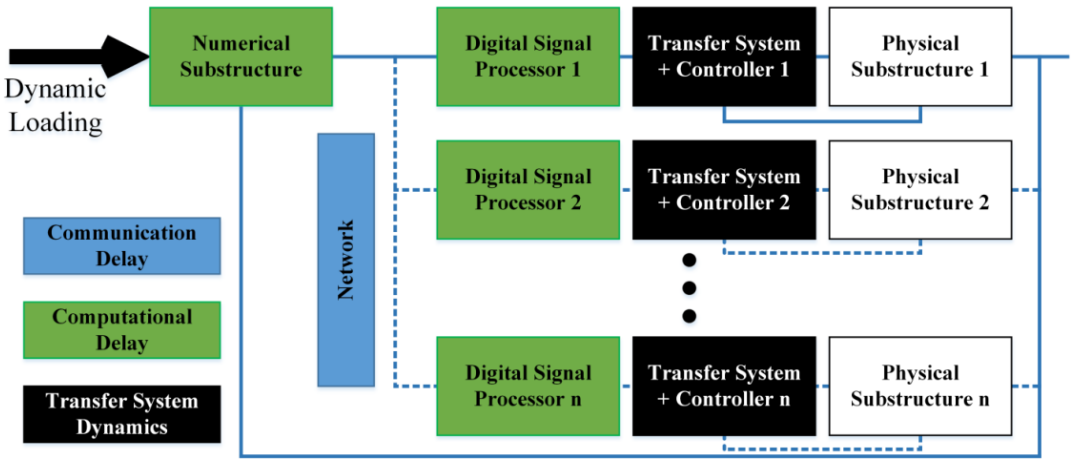

Fig. 2 General distributed RTHS architecture

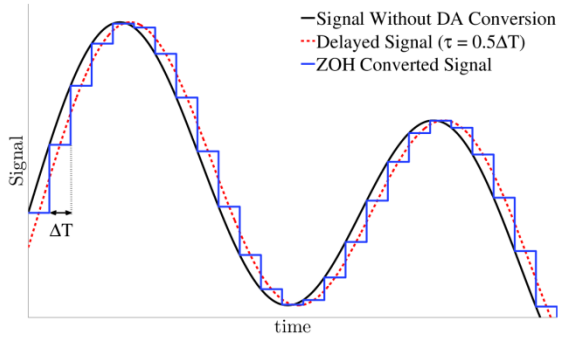

Fig. 3 ZOH digital-to-analog conversion

Fig. 4 Servo-hydraulic actuator as a common transfer system

2.2 Computational delay

In RTHS, integration schemes are implemented to solve the discretized governing equation of the numerical substructure. Stability and performance issues are limiting factors which determine the maximum permissible computational time and the largest natural frequency of the numerical model in a linear case. In RTHS, all computations are executed on processors and then the command signal is implemented using a digital-to-analog convertor (DAC). One of the most common methods is the zero-order hold method (ZOH) shown in Fig. 3. It has been shown that the effect of the ZOH conversion on the signal is approximately equal to that of a time delay of $0.5\Delta T = (2f_s)^{-1}$where f_s and ΔT are the sampling frequency and time interval, respectively, see (Maghareh and Dyke 2013).

2.3 Transfer system dynamics

Experimental studies have shown that no matter which control strategy is adopted, there is always a time lag between the command input and the realization of the command by the transfer system which is often frequency dependent. Dyke *et al*. analyzed the effects of control-structure interaction (CSI) and demonstrated that the dynamics of a hydraulic actuator, a common type of transfer system in RTHS, and the plant are coupled through a natural velocity feedback. So, the time lag is caused by both actuator dynamics and the attached specimen (Dyke *et al*. 1995) and is

not a pure time delay. However, the contribution of the actuator dynamics is dominant (Zhao *et al*. 2003) and within a typical seismic frequency bandwidth, experimental studies have demonstrated that a linearized actuator model can capture the essential dynamics of the actuator (Gao 2012). Typically, the natural frequency of the attached specimen in RTHS is large compared to the seismic frequency bandwidth. Therefore, under certain conditions, the phase of the actuator frequency response function can be approximated as linear and modeled as a pure time delay (Carrion and Spencer 2007). Typical values for actuator time lags reported in the literature range from 8 to 30 msec. (Horiuchi *et al*. 1999, Darby *et al*. 2002, Shing *et al*. 2004).

2.4 Time delay and system dynamics (or Time Lag)

Time delay and system dynamics are two different concepts which are sometimes used interchangeably. To delineate the difference, this work compares the dynamics of a servo-hydraulic actuator model with a time delay system in the frequency domain. A time delay system and a linear system dynamics can be mathematically expressed as

$$x(t) = u(t-\tau) \tag{6a}$$

$$x^{(n)}(t) + \cdots + a_0 x(t) = b_m u^{(m)}(t) + \cdots + b_0 \tag{6b}$$

where $u(t)$, $x(t)$ and τ are the system input, system output and time delay value, respectively.

A very common type of transfer system in RTHS is a servo-hydraulic actuator. For a more realistic comparison, the servo-hydraulic actuator shown in Fig. 4 was identified at the Intelligent Infrastructure System Lab at Purdue University. The identified dynamics of the servo-hydraulic actuator, which corresponds to measured displacement to command displacement, is given by

$$\frac{x_{msd}(s)}{x_{cmd}(s)} = \frac{2.382\times10^9}{s^4+485.5s^3+1.317\times10^5 s^2+3.182\times10^7 s+2.382\times10^9} \tag{7}$$

where $s \in \mathbb{C}$ is the Laplace variable. Fig. 5 provides the frequency responses of the servo-hydraulic actuator and a pure time delay system.

$$[M_n]\ddot{x}(t) + [C_n]\dot{x}(t) + R_n(x) = -[M]\Gamma\ddot{x}_g(t) - F_{fb}(t-\tau) \tag{8a}$$

$$F_{fb}(t) = [M_p]\ddot{x}(t) + [C_p]\dot{x}(t) + R_p(x) \tag{8b}$$

Clearly, over a relatively low frequency bandwidth, the responses of the pure time delay and transfer system dynamics are quite similar. In RTHS, the frequency bandwidth of interest is the seismic frequency bandwidth and it is restricted to a low frequency bandwidth. Therefore, over a relatively low frequency bandwidth, we can model the dynamic interaction of a transfer system and the physical substructure with a constant time delay (Christenson *et al*. 2008, Maghareh *et al*. 2012). Thus, in this study, Eq. (5) is replaced by Eqs. (8(a)) and (8(b)) in which the communication delay, computational delay, and transfer system dynamics are all lumped into a single time delay (τ) which acts upon the feedback restoring force signal.

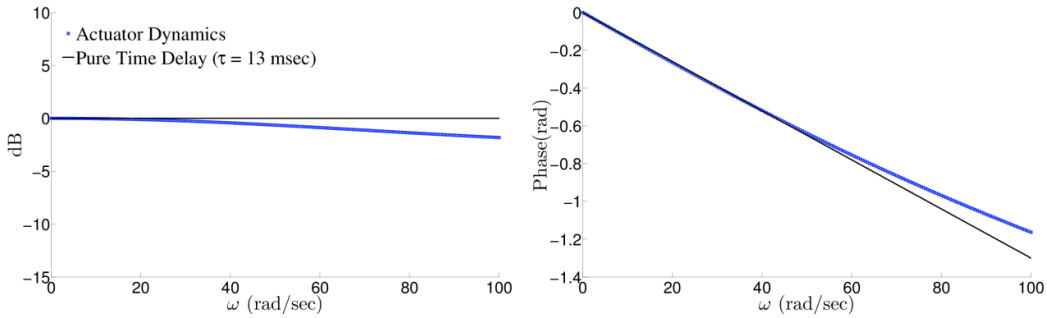

Fig. 5 Frequency responses of the servo-hydraulic actuator model and a pure time delay system

3. An RTHS stability switch criterion

To conduct a stability analysis of linear RTHS systems, a general geometric stability switch criterion in delay differential systems can be implemented to establish an RTHS stability switch criterion. A more detailed discussion on the general geometric stability switch criterion is provided in (Wallace *et al*. 2005, Beretta and Kuang 2002). Consider a linear single-degree-of-freedom (SDOF) reference structure with a seismic excitation, as follows

$$M\ddot{x}(t) + C\dot{x}(t) + Kx = -M\ddot{x}_g(t) \tag{9}$$

where M, C,and K are the reference structure's mass, damping, and stiffness, respectively. For SDOF RTHS, the reference structure is partitioned into numerical and physical substructures, as shown in Fig. 6. The governing equation of the SDOF RTHS shown in Fig. 6 is

$$M_n\ddot{x}(t) + C_n\dot{x}(t) + K_n x = -M\ddot{x}_g(t) - F_{fb}(t-\tau) \tag{10a}$$

$$F_{fb}(t) = M_p\ddot{x}(t) + C_p\dot{x}(t) + K_p x \tag{10b}$$

To study the response of this RTHS system, we use the Laplace transform in which

$$\mathcal{L}[\dots](s) = \int_{-\infty}^{\infty} \dots e^{-st}\, dt \tag{11}$$

In the Laplace domain, the response of the reference structure, Eq. (9), is given by

$$x_{REF}(s) = \frac{-M}{Ms^2+Cs+K}\ddot{x}_g(s) \tag{12}$$

In the absence of a feedback time delay ($\tau = 0$), the response of the RTHS system, Eq. (10(a)), can be expressed as

$$x_{RTHS}(s) = \frac{-M}{M_n s^2+C_n s+K_n}\ddot{x}_g(s) - \frac{M_p s^2+C_p s+K_p}{M_n s^2+C_n s+K_n}x_{RTHS}(s) \tag{13}$$

therefore

$$\frac{Ms^2+Cs+K}{M_n s^2+C_n s+K_n}x_{RTHS}(s) = \frac{-M}{M_n s^2+C_n s+K_n}\ddot{x}_g(s) \tag{14}$$

and

$$x_{RTHS}(s) = x_{REF}(s) = \frac{-M}{Ms^2+Cs+K}\ddot{x}_g(s) \tag{15}$$

Thus, in the absence of feedback time delay, the response of an RTHS system, Eq. (10(a)) is identical to the response of the reference structure, Eq. (9). However, in the presence of feedback time delay, the response of the RTHS system in Eq. (10(a)) takes the Laplace transform of

$$x_{RTHS}(s) = \frac{-M}{(M_n s^2+C_n s+K_n)+(M_p s^2+C_p s+K_p)e^{-\tau s}}\ddot{x}_g(s) \tag{16}$$

and the resulting characteristic equation is written as

$$\Gamma(\lambda,\tau) = (M_n\lambda^2 + C_n\lambda + K_n) + \left(M_p\lambda^2 + C_p\lambda + K_p\right)e^{-\tau\lambda} \tag{17}$$

where $\Gamma \in \mathbb{C}$. Eq. (17) can be expressed as

$$\Gamma(\lambda,\tau) = \Gamma_n(\lambda) + \Gamma_p(\lambda)e^{-\tau\lambda} \tag{18}$$

For a dynamic system to be asymptotically stable about its fixed points, all eigenvalues, which are the roots of the corresponding characteristic equation, must lie in the left half of the complex plane. Therefore, stability switching occurs when a root of the characteristic equation crosses the imaginary axis (i.e., $\mathrm{Re}(\lambda_i) = 0$) as some parameters vary in the characteristic equation. If the partitioning parameters of the RTHS are chosen such that any root of the characteristic equation is in the right half of the complex plane, then that test configuration will be unstable.

Without loss of generality, it is assumed that the reference structure ($\tau = 0$) is stable (i.e., the roots of $\Gamma(\lambda, 0)$ in Eq. (18) lie in the left half of the complex plane). Next, we introduce two new terms which are crucial in the theory of delay differential equations: (1) critical frequency ($\omega_{cr} = |\lambda_{cr}|$) which is the frequency at which a stability switch occurs, and (2) critical time delay (τ_{cr}) which is the time delay associated with the occurrence of a stability switch. To obtain the critical frequency and critical time delay associated with Eq. (18), one can simply replace λ, τ with $j\omega_{cr}$, τ_{cr} in Eq. (18), and express the characteristic equation as

$$-\frac{\Gamma_n(j\omega_{cr})}{\Gamma_p(j\omega_{cr})} = e^{-j\tau_{cr}\omega_{cr}} = e^{-j\Omega_{cr}} \tag{19}$$

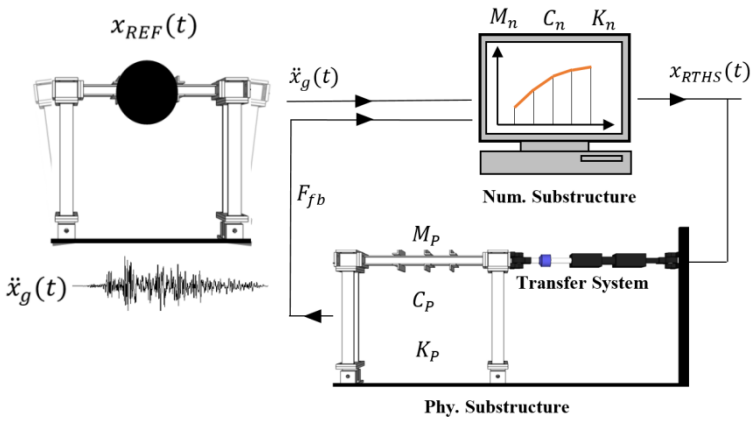

Fig. 6 Schematic diagram of a SDOF RTHS

where j is the imaginary unit number and ω_{cr} is the product of the critical frequency and its corresponding critical time delay $\Omega_{cr} = \tau_{cr}\omega_{cr}$. Eq. (19) can be solved using the geometric construction presented in (MacDonald 1989). As Ω_{cr} increases from 0 to 2π, $e^{-j\Omega_{cr}}$ traces out a unit circle in the complex plane and the left hand side of the equation, which is called *the ratio curve*, traces out another curve. A stability switch occurs in the system when the unit circle intersects the ratio curve. The intersection can occur multiple times, meaning that the system is stable within a particular range of time delay, then it will be unstable for a specific range of time delay, and then the system may gain its stability back as the time delay increases, see Fig. 7. For RTHS, the first occurrence of the instability condition is the most meaningful. Using Eqs. (17)-(19) the characteristic equation of a SDOF RTHS can be expressed as

$$-\frac{-M_n{\omega_{cr}}^2+C_n\omega_{cr}j+K_n}{-M_p{\omega_{cr}}^2+C_p\omega_{cr}j+K_p} = e^{-j\tau_{cr}\omega_{cr}} \tag{20}$$

Using Euler's formula (i.e., $e^{\cdots j} = \cos \ldots + j \sin \ldots$), Eq. (20) can be written as

$$\begin{aligned}&[-M_n\omega_{cr}^2 + C_n\omega_{cr}j + K_n]\\&+\left[-M_p\omega_{cr}^2 + C_p\omega_{cr}j + K_p\right][cos(\tau_{cr}\omega_{cr}) - jsin(\tau_{cr}\omega_{cr})] = 0\end{aligned} \tag{21}$$

Separating the real and imaginary parts of Eq. (21) yields the following system of equations,

$$\left[K_p - M_p\omega_{cr}^2\right]cos(\tau_{cr}\omega_{cr}) + C_p\omega_{cr}sin(\tau_{cr}\omega_{cr}) = M_n\omega_{cr}^2 - K_n \tag{22a}$$

$$C_p\omega_{cr}cos(\tau_{cr}\omega_{cr}) - \left[K_p - M_p\omega_{cr}^2\right]sin(\tau_{cr}\omega_{cr}) = -C_n\omega_{cr} \tag{22b}$$

Dividing both sides of Eqs. (22(a)) and (22(b)) by M yields

$$\begin{cases}[(1-\gamma)\omega_n^2 - (1-\alpha)\omega_{cr}^2]cos(\tau_{cr}\omega_{cr}) + [2(1-\beta)\omega_{cr}\zeta\omega_n]sin(\tau_{cr}\omega_{cr})\\ = \alpha\omega_{cr}^2 - \gamma\omega_n^2\end{cases} \tag{23a}$$

$$\begin{cases}[2(1-\beta)\omega_{cr}\zeta\omega_n]cos(\tau_{cr}\omega_{cr}) - [(1-\gamma)\omega_n^2 - (1-\alpha)\omega_{cr}^2]sin(\tau_{cr}\omega_{cr})\\ = -2\omega_n\zeta\omega_{cr}\beta\end{cases} \tag{23b}$$

where $\{\alpha, \beta, \gamma\} = \{M_nM^{-1},\ C_nC^{-1}, K_nK^{-1}\}$ are the partitioning parameters and ζ is damping ratio. Eqs. (23(a)) and (23(b)) are squared and added together to obtain a 4$^{\text{th}}$order equation governing how the partitioning factors and the structural characteristics of the reference structure determine the critical frequency of the RTHS system (ω_{cr})

$$(1-2\alpha)\omega_{cr}^4 + \omega_n^2[4(1-2\beta)\zeta^2 - 2(1-\alpha-\gamma)]\omega_{cr}^2 + (1-2\gamma)\omega_n^4 = 0 \tag{24}$$

Furthermore, Eq. (24) is normalized with respect to ω_n yielding

$$(1-2\alpha)\phi_{cr}^4 + [4(1-2\beta)\zeta^2 - 2(1-\alpha-\gamma)]\phi_{cr}^2 + (1-2\gamma) = 0 \tag{25}$$

where $\phi_{cr} = \omega_{cr}\omega_n^{-1}$ is the critical frequency ratio. Eq. (25) may lead to 0, 1, or 2 meaningful critical frequencies (i.e., positive real values). The lowest of the three is associated with the limit of an unconditionally stable RTHS system. After obtaining ϕ_{cr} from Eq. (25), one can solve for the corresponding critical time delays using Eqs. (23(a)) and (23(b))

$$\tau_{cr} = {\omega_{cr}}^{-1}\left[N\pi + tan^{-1}\left(\frac{A}{B}\right)\right] \tag{26a}$$

$$A = [2(1-\beta)\omega_{cr}\zeta\omega_n][\alpha\omega_{cr}^2 - \gamma\omega_n^2] + [(1-\gamma)\omega_n^2 - (1-\alpha)\omega_{cr}^2]2\omega_n\zeta\omega_{cr}\beta \tag{26b}$$

$$B = [(1-\gamma)\omega_n^2 - (1-\alpha)\omega_{cr}^2][\alpha\omega_{cr}^2 - \gamma\omega_n^2] - [2(1-\beta)\omega_{cr}\zeta\omega_n]2\omega_n\zeta\omega_{cr}\beta \tag{26c}$$

where $N = 0, 1, 2, ...$ and making sure that Eqs. (23(a)) and (23(b)) are both achieved. Furthermore, Eq. (26) is normalized with respect to ω_n and it becomes

$$\Omega_{cr} = \tau_{cr}\omega_n = {\phi_{cr}}^{-1}\left[N\pi + tan^{-1}\left(\frac{A}{B}\right)\right] \tag{27a}$$

$$A{\omega_n}^{-4} = [2(1-\beta)\phi_{cr}\zeta][\alpha\phi_{cr}^2 - \gamma] + [(1-\gamma)\omega_n^2 - (1-\alpha)\phi_{cr}^2]2\zeta\phi_{cr}\beta \tag{27b}$$

$$B{\omega_n}^{-4} = [(1-\gamma) - (1-\alpha)\phi_{cr}^2][\alpha\phi_{cr}^2 - \gamma] - [2(1-\beta)\phi_{cr}\zeta]2\phi_{cr}\zeta\beta \tag{27c}$$

Thus, Eqs. (25) and (27(a)) can be used to find the stability characteristics of an RTHS system as a function of the partitioning parameters and the structural characteristics of the reference structure. However, it is recommended to first plot the RTHS stability diagram using Eqs. (25) and (27a), and then determine the stability characteristics of the RTHS system.

3.1 Stability diagrams for a linear SDOF RTHS

This section examines how the values of the partitioning parameters and the structural characteristics of the reference structure affect the stability of a linear RTHS system through the use of RTHS stability diagrams. Four sample partitioning cases will be considered, see Table 1. In Fig. 7, the stability diagrams associated with these sample cases, for 5 different reference damping ratios (a total of 4 × 5 = 20 systems) are examined.

Practically speaking, a more realistic partitioning configuration is one where a majority of the mass is modeled in the numerical substructure (i.e., $\alpha \approx 1$) and a majority of the stiffness is placed in the physical substructure (i.e., $\gamma \approx 0$). Therefore, the bottom portion of Fig. 7(b) and the top portion of Fig. 7(c) represent more realistic scenarios. As shown in Fig. 7, the more realistic cases where $\alpha \approx 1$ and $\gamma \approx 0$ are quite challenging configurations in terms of leading to small values of Ω_{cr}. Some important observations can be made from Fig. 7.

- For a specific ζ, the area to the left of the first curve is considered a stable region in RTHS (i.e., $\Omega < \Omega_{cr}$).
- The critical time delay is inversely proportional to the natural frequency of the reference structure. Thus, higher modes of the reference structure are highly sensitive to time delays. Often for multi-degree-of-freedom (MDOF) systems, higher modes are suppressed with artificial damping in the numerical substructure (Shing and Mahin 1984).

Table 1 The four partitioning cases examined

	α factor	β factor	γ factor
Case I	$\in [0, 1]$	0.4	0.9
Case II	0.9	0.6	$\in [0, 1]$
Case III	$\in [0, 1]$	0.6	0.1
Case IV	0.1	0.4	$\in [0, 1]$

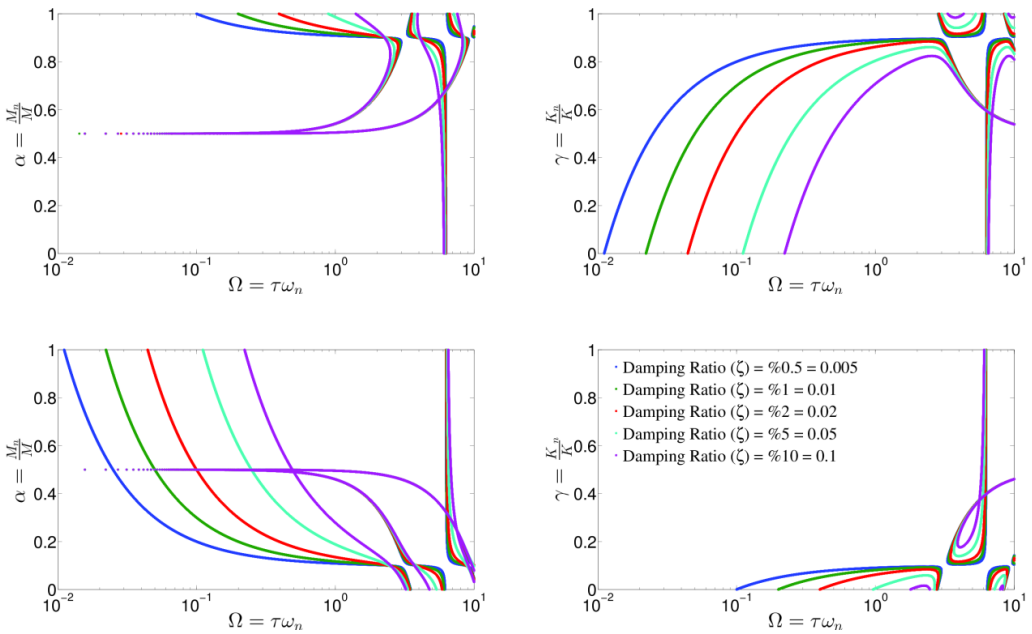

Fig. 7 Normalized stability diagrams showing Ω_{cr} (a) Case I (b) Case II (c) Case III (d) Case IV

- In selecting the partitioning parameters, $\alpha \approx 0.5$ is not a good choice from stability and performance perspectives, see Figs. 7(a) and 7(c).
- For a particular RTHS configuration, multiple Ω_{cr}(s) exist. Clearly, a stability switch occurs in the system when the unit circle in Eq. (19) intersects the ratio curve, and this can occur multiple times. Thus, the system is stable within a particular range of Ω, then it will be unstable for a specific range of Ω, and then the system will again be stable as Ω increases. Although the system may be stable at higher Ω, performance is likely to suffer (Maghareh *et al*. 2013)
- As a rule of thumb, the value of critical time delay is related to $|\gamma - \alpha|$. Thus, larger value of $|\gamma - \alpha|$ usually leads to a relatively small critical time delay value.
- Critical time delay usually increases as the reference structure becomes more damped.
- Finally, if stability concerns lead to some changes in a partitioning setup, reducing $|\gamma - \alpha|$ and ω_n and/or increasing ζ are effective options.

3.2 Unconditionally stable region

As noted earlier, Eq. (25) may lead to 0, 1, or 2 meaningful critical frequency ratios. For case II and $\zeta = 5\%$, these three regions are shown in Fig. 8. Using Eq. (25), the condition to have an unconditionally stable region is

$$(\gamma - \alpha) < 4\zeta^2(1 - 2\beta)[(1 - \alpha - \gamma) - (1 - 2\beta)\zeta^2] \tag{28}$$

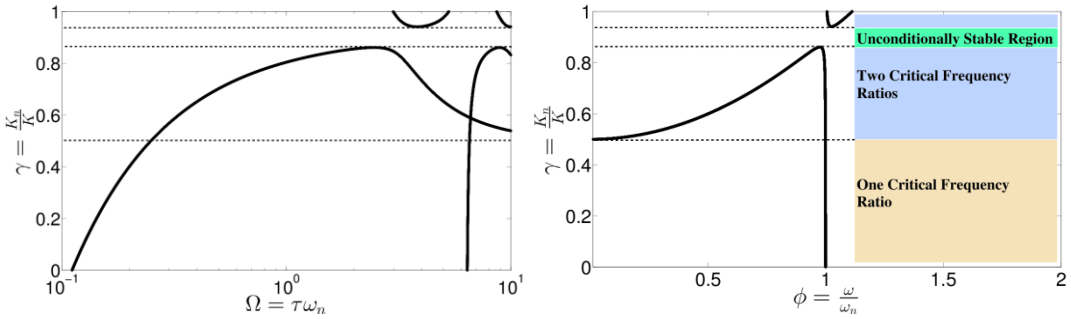

Fig. 8 Case II with $\zeta = 5\%$ (a) Normalized RTHS stability diagram showing Ω_{cr} against γ (b) Plot of γ against Φ_{cr} showing the three stability regions

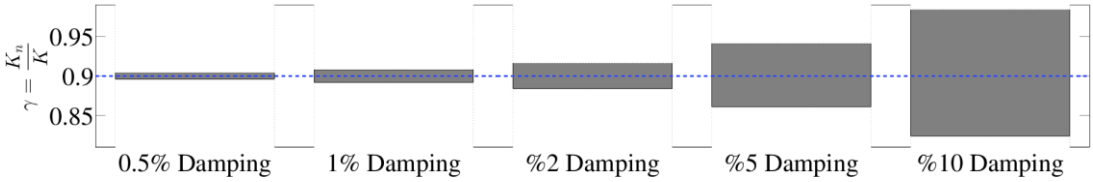

Fig. 9 Unconditionally stable range associated with case II for different damping ratios

Moreover, in terms of α and γ, the range of the unconditionally stable region, which occurs about $|\gamma - \alpha| = 0$, can be found as

$$(\gamma - \alpha)^2 + B(\gamma - \alpha) + C = 0 \tag{29}$$

where $B = 4(1 - 2\beta)\zeta^2$ and $C = -4\zeta^2(1 - 2\beta)[1 - 2\alpha - (1 - 2\beta)\zeta^2]$. Fig. 9 shows the resulting unconditionally stable range associated with Case II about $|\gamma - \alpha| = 0$ using Eq. (29).

Thus, in certain RTHS configurations, there is a range about $|\gamma - \alpha| = 0$ in which the system is unconditionally stable, and within that range, the critical time delay approaches infinity. Knowing the unconditionally stable region associated with a partitioning set-up can be significant, especially when conducting geographically-distributed RTHS where data loss and unpredictable time delays are major challenges.

3.3 Minimum requirements of the transfer system and sampling frequency

After obtaining the critical time delay using the RTHS stability diagrams or Eqs. (25) and (27(a)), one can identify the maximum permissible delay in an RTHS system as the critical time delay. Therefore, if the feedback force signal has a time delay equal to or greater than the critical time delay, the system will go unstable. Generally speaking, the time delay associated with the feedback force signal is

$$\tau_{Ffb} = \tau_{COMP} + \tau_{COMM} + \tau_{TS} \tag{30}$$

where τ_{COMP}, τ_{COMM}, and τ_{TS} are computational delay, communication delay, transfer system

delay, respectively. Furthermore, if a ZOH digital-to-analog convertor is used, τ_{COMP} can be approximated by $(2f_s)^{-1}$ where f_s is the sampling frequency in Hz. Assuming that in a local RTHS, τ_{COMM} is a known deterministic value. Then, Eq. (30) becomes

$$\tau_{Ffb} - \tau_{COMM} - (2f_s)^{-1} = \tau_{TS} \tag{31}$$

therefore, with a given sampling frequency, the stability phase envelope which determines the minimum control requirements for the transfer system can be expressed as

$$e^{-j\omega(\tau_{cr}-\tau_{COMM}-(2f_s)^{-1})} = e^{-j\omega\tau_m} \tag{32}$$

where $\tau_m = \tau_{cr} - \tau_{COMM} - (2f_s)^{-1}$. As shown in Fig. 10, for a stable RTHS, the phase plot of the transfer system control must lie above the stability phase envelope shown for a given value of τ_{cr}.

4. Weakly-nonlinear SDOF RTHS systems

This section considers a physical substructure that is composed of weakly-nonlinear materials (wherein there is a nonlinearity between the materials' restoring forces and displacements) or composed of linear materials but loaded beyond the proportional limit. Let's examine how nonlinearity affects the overall stability of a SDOF RTHS system in the presence of feedback time delay. Consider a lightly-damped reference structure with the following governing equation

$$M\ddot{x}(t) + C\dot{x}(t) + Kx(t) + \epsilon R(x) = 0 \tag{33}$$

which is equivalent to

$$\ddot{x}(t) + 2\zeta\omega_n\dot{x}(t) + {\omega_n}^2 x(t) + \epsilon M^{-1}R(x) = 0 \tag{34}$$

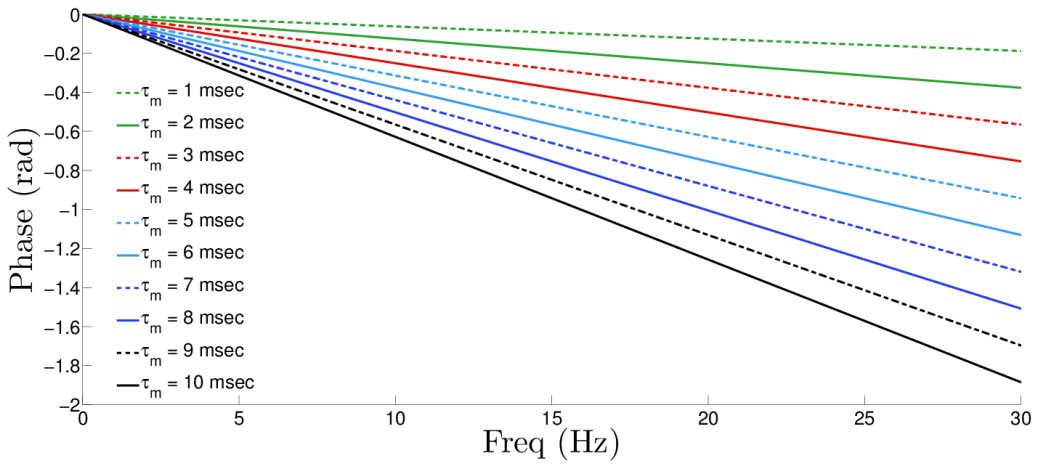

Fig. 10 Stability phase envelope to determine the minimum transfer system control requirement

where $\epsilon R(x)$ represents the weakly-nonlinear component of the restoring force and ϵ is a small positive constant (ϵ and $\zeta$are in the same order of magnitude). Weakly-nonlinear systems can be divided into two categories: (1) strain-hardening systems and (2) strain-softening systems. Fig. 11 shows the qualitative behaviors of linear, strain-softening, and strain-hardening systems. In this work, we assume that these nonlinearities can be captured with cubic terms. Thus, Eq. (34) becomes

$$\ddot{x}(t) + 2\zeta\omega_n\dot{x}(t) + {\omega_n}^2 x(t) + \epsilon M^{-1} h x^3(t) = 0 \tag{35}$$

where $\{h < 0, h = 0, h > 0\}$ corresponds to {strain-softening, linear, strain-hardening} systems. Eq. (35) can be partitioned into numerical and physical substructures using the partitioning parameters, $\{\alpha, \beta, \gamma\} = \{M_n M^{-1},\ C_n C^{-1}, K_n K^{-1}\}$, yielding

$$\begin{aligned} &\{\alpha\ddot{x}(t) + 2\zeta\beta\omega_n\dot{x}(t) + \gamma{\omega_n}^2 x(t)\} \\ &+\{(1-\alpha)\ddot{x}(t) + 2\zeta(1-\beta)\omega_n\dot{x}(t) + (1-\gamma){\omega_n}^2 x(t) + \epsilon M^{-1} h x^3(t)\} = 0 \end{aligned} \tag{36}$$

where in the presence of feedback delay, Eq. (36) becomes

$$\begin{aligned} &\{\alpha\ddot{x}(t) + 2\zeta\beta\omega_n\dot{x}(t) + \gamma{\omega_n}^2 x(t)\} \\ &+\{(1-\alpha)\ddot{x}(t-\tau) + 2\zeta(1-\beta)\omega_n\dot{x}(t-\tau) + (1-\gamma){\omega_n}^2 x(t-\tau)\} \\ &+\{\epsilon M^{-1} h x^3(t-\tau)\} = 0. \end{aligned} \tag{37}$$

For a SDOF RTHS system, it has been shown that the presence of a feedback time delay effectively adds energy into the system (Ahmadizadeh 2007, Mosqueda *et al*. 2005, Carrion and Spencer 2007). Fig. 12 shows desired displacement against the restoring forces of linear and weakly-nonlinear systems associated with different time delays, where $\tau_1 < \tau_2 < \tau_3$. In each case, the additional energy added to the system is the enclosed area. Clearly, as the time delay becomes larger, the effective amount of added energy increases.

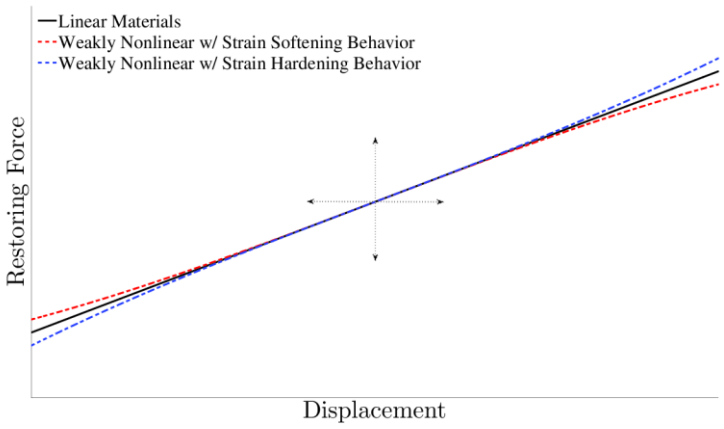

Fig. 11 Qualitative behavior of linear, strain-softening, and strain-hardening materials

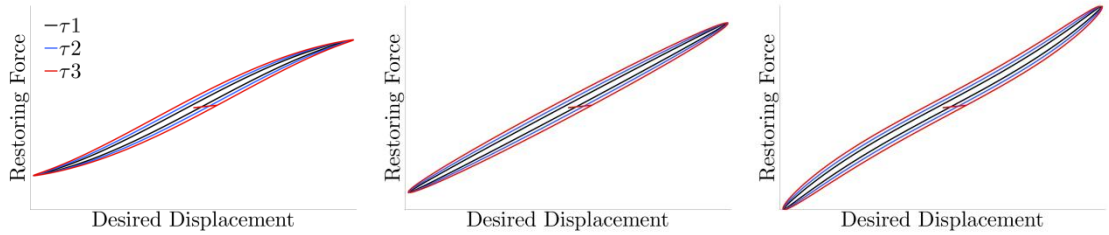

Fig. 12 Additional energy due to time delay in strain-softening, linear and strain-hardening systems $(\tau_1 < \tau_2 < \tau_3)$

For RTHS, instability occurs when the additional energy becomes greater than the energy dissipation in the nominal system (and hysteretic energy if any) (Ahmadizadeh 2007). Using the stability switch criterion, we can obtain the critical time delay associated with the linear system, and the qualitative effects of weak nonlinearity on the stability of the system can be understood by computing and comparing the enclosed areas shown in Fig. 12.

Linear Systems: In Eq. (37), linear systems correspond to systems with $h = 0$. Therefore, the enclosed area in Fig. 12(b), can be computed as

$$A_L(t) = \int_{x(t_o)}^{x(t_1)} (1-\gamma)K[x(t) - x(t-\tau)]\, dx \tag{38a}$$

$$= \int_{t_o}^{t_1} (1-\gamma)K[x(t) - x(t-\tau)]\, \dot{x}(t) dt \tag{38b}$$

Strain-Softening Systems: In Eq. (37), strain-softening systems correspond to systems with $h < 0$. Therefore, the enclosed area in Fig. 12(a) can be computed as

$$A_s(\tau) = \int_{x(t_o)}^{x(t_1)} \{(1-\gamma)K[x(t) - x(t-\tau)] + \epsilon h[x^3(t) - x^3(t-\tau)]\}\, dx \tag{39a}$$

$$A_s(\tau) = \int_{t_o}^{t_1} [x(t) - x(t-\tau)]\{(1-\gamma)K + \epsilon h[x^2(t) + x(t)x(t-\tau) + x^2(t-\tau)]\}\dot{x}(t) dt \tag{39b}$$

by applying the Taylor expansion on $[x(t) - x(t-\tau)]$ and truncating $o(\tau^2)$, $[x(t) - x(t-\tau)]$ can be approximated as $\tau\dot{x}(t)$, yielding

$$A_s(\tau) = \int_{t_o}^{t_1} (1-\gamma)K[x(t) - x(t-\tau)]\dot{x}(t) dt + \int_{t_o}^{t_1} \epsilon h\tau[x^2(t) + x(t)x(t-\tau) + x^2(t-\tau)]\, \dot{x}^2(t) dt \tag{40a}$$

$$A_S(\tau) = A_L(\tau) + \Delta A_S(\tau) \tag{40b}$$

Knowing that $\forall\{x(t), \tau\}$ and $\epsilon h\tau < 0$: $\epsilon h\tau[x^2(t) + x(t)x(t-\tau) + x^2(t-\tau)]\dot{x}^2(t) \leq 0$ yields

$$\Delta A_S(\tau) \leq 0 \tag{41a}$$

$$A_S(\tau) \leq A_L(\tau) \tag{41b}$$

Thus, the enclosed area in Fig. 12(a) (i.e., the additional energy for strain-softening systems) is always smaller than the enclosed area in Fig. 12(b) (i.e., the additional energy for linear systems).

Strain-Hardening Systems: In Eq. (37), strain-hardening systems correspond to systems with $h > 0$. Therefore, the enclosed area in Fig. 12(c) can be computed as

$$A_H(\tau) = \int_{x(t_o)}^{x(t_1)} \{(1-\gamma)K[x(t) - x(t-\tau)] + \epsilon h[x^3(t) - x^3(t-\tau)]\}\, dx \tag{42a}$$

$$\begin{aligned} A_H(\tau) = \int_{t_o}^{t_1} [x(t) - x(t-\tau)]\{(1-\gamma)K + \\ \epsilon h[x^2(t) + x(t)x(t-\tau) + x^2(t-\tau)]\}\dot{x}(t)dt \end{aligned} \tag{42b}$$

by applying the Taylor expansion on $[x(t) - x(t-\tau)]$ and truncating $o(\tau^2), [x(t) - x(t-\tau)]$ can be approximated as $\tau\dot{x}(t)$, yielding

$$\begin{aligned} A_H(\tau) = \int_{t_o}^{t_1} (1-\gamma)K[x(t) - x(t-\tau)]\dot{x}(t)dt \\ + \int_{t_o}^{t_1} \epsilon h\tau[x^2(t) + x(t)x(t-\tau) + x^2(t-\tau)]\, \dot{x}^2(t)dt \end{aligned} \tag{43a}$$

$$A_H(\tau) = A_L(\tau) + \Delta A_H(\tau) \tag{43b}$$

Knowing that $\forall\{x(t), \tau\}$ and $\epsilon h\tau > 0: \epsilon h\tau[x^2(t) + x(t)x(t-\tau) + x^2(t-\tau)]\dot{x}^2(t) \geq 0$ yields

$$\Delta A_H(\tau) \geq 0 \tag{44a}$$

$$A_H(\tau) \geq A_L(\tau) \tag{44b}$$

Thus, the enclosed area in Fig. 12(c) (i.e., the additional energy for strain-hardening systems) is always larger than the enclosed area in Fig. 12b (i.e. the additional energy for linear systems). In Fig. 12(b), for a given τ, $A_S(\tau)$, $A_L(\tau)$, and $A_H(\tau)$ are compared, and clearly

$$A_H(\tau) \geq A_L(\tau) \geq A_S(\tau) \tag{45}$$

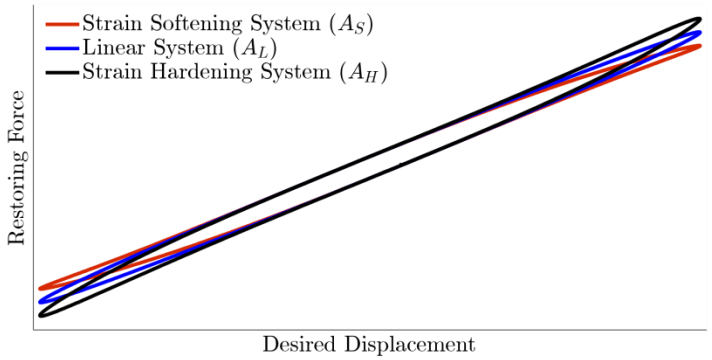

Fig. 13 Comparison of additional energies added to the system due to time delay in the restoring force

For weakly-nonlinear systems, the system can be linearized about its fixed point and using the RTHS stability switch criterion, a value for critical time delay can be obtained. However, it should be noted that depending upon whether the system exhibits softening or hardening behavior, the obtained value is underestimated or overestimated, respectively. Therefore, for weakly-nonlinear systems with softening behavior, the obtained value is a conservative value. Furthermore, $A_L(\tau) - A_S(\tau)$ and $A_H(\tau) - A_L(\tau)$ are linearly proportional to $\epsilon h \tau$. Thus, the level of nonlinearity and damping of the reference structure determine the level of overestimation or underestimation of the critical time delay value obtained using the RTHS stability switch criterion.

5. Illustrative case studies

To illustrate the use of the RTHS stability switch criterion, we conducted experimental and numerical studies. In the first section, the results associated with a pure physical (shake table) testing of a reference structure, simulation of the reference model, and RTHS are provided. In the latter section, two simulations of RTHS (case a and case b) are provided.

5.1 Illustrative experiment

In this section, we conduct a pure physical (shake table) testing of a SDOF structure (i.e., the reference structure), a simulation of the reference structure (i.e., the reference model), and an RTHS (experimental case). The objective is to utilize the RTHS stability switch criterion and predictive stability/performance indicators (PSI and PPI), established in (Maghareh *et al*. 2013, Maghareh and Dyke 2013), to conduct a successful RTHS where: (1) the transfer system (i.e., a servo hydraulic actuator) is controlled (or compensated) relatively poorly (i.e., poor transfer system performance), see Fig. 16; (2) the reference structure has a relatively large natural frequency ($\omega_n = 32.9\, rad/sec$) and is lightly damped ($\zeta = 0.014$). For RTHS, it is quite challenging to conduct a successful RTHS where $\Omega = \tau\omega_n$ is relatively large and ζ is relatively small.

In this study the seismic input is chosen to be the ChiChi earthquake ground acceleration and the peak ground acceleration is scaled to be 0.061g, see Fig. 14. To begin, a comparison is made between the shake table response of the reference structure and the response of its SDOF reference model. This step is necessary to obtain reliable values for $\{M, C, K\}_{REF}$ and eventually $\{\alpha, \beta, \gamma\}$. Fig. 15 shows the response of the reference structure and the reference model in the time and frequency domains. The corresponding normalized RMS error (NRMSE) using Eq. (46) is 0.8%.

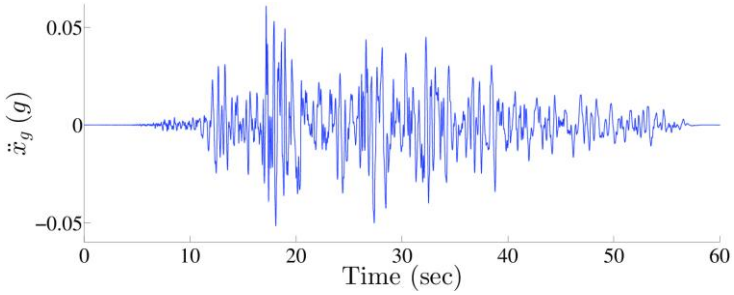

Fig. 14 ChiChi earthquake ground acceleration with PGA = 0.061g

$$NRMSE\% = \frac{RMS[\ddot{x}_{PHY}(t) - \ddot{x}_{SIM}(t)]}{max[\ddot{x}_{PHY}(t)] - min[\ddot{x}_{PHY}(t)]} \times 100 \quad (46)$$

A low NRMSE and excellent agreement in Fig. 15 show that the reference structure is accurately modeled. After identifying the reference structure, we are ready to partition the reference structure and utilize the RTHS stability switch criterion, the PSI and PPI. The structural characteristics of the reference structure, the physical substructure, and the numerical substructure are listed in Table 2. Therefore, for this RTHS system, $\{\zeta, \omega_n, \alpha, \beta, \gamma\} = \{1.37\%, 32.9\ rad/sec, 0.75, 0.82, 0.75\}$ are a good choice of parameters.

Next, to conduct RTHS, we first evaluate the performance of the transfer system. In Fig. 16, the frequency responses of the hydraulic actuator identified using band-limited white noise input and a pure time delay system are shown. Furthermore, in the RTHS setup shown in Fig. 17, $\{f_s, \tau_{COMP}, \tau_{COMM}, \tau_{TS}\}$ is $\{4096\ Hz, 0.12\ msec, 0.24\ msec, 14.4\ msec\}$. Thus, the feedback time delay can be approximated as 14.8 msec. By knowing τ, ω_n, and the partitioning parameters, one can locate the corresponding RTHS case on the RTHS stability diagram. In Fig. 18, the case is specified with a blue cross-mark and labeled as RTHS (Experimental Case). Using the predictive indicators, one can predict that the partitioning choice in Table 2 and $\Omega = 0.49$ leads to unconditionally stable (PSI = ∞) and accurate results (PPI = 0.205), see (Maghareh and Dyke 2013, Maghareh *et al*. 2013).

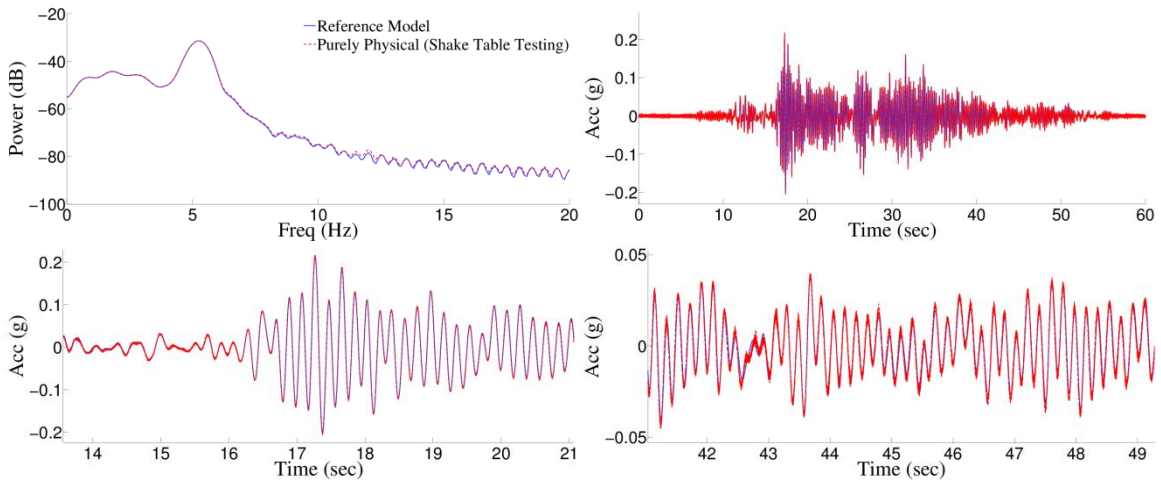

Fig. 15 Responses of pure physical (shake table) testing and the SDOF reference model, (a) frequency domain, (b) time domain, (c) time domain (zoomed in), (d) time domain (zoomed in)

Table 2 Reference and substructures characteristics

	Reference	Physical	Numerical
M (kg)	98.4	24.6	73.8
C (N.s/m)	88.7	15.8	72.9
K(N/m)	10.67e4	2.67e4	8e4

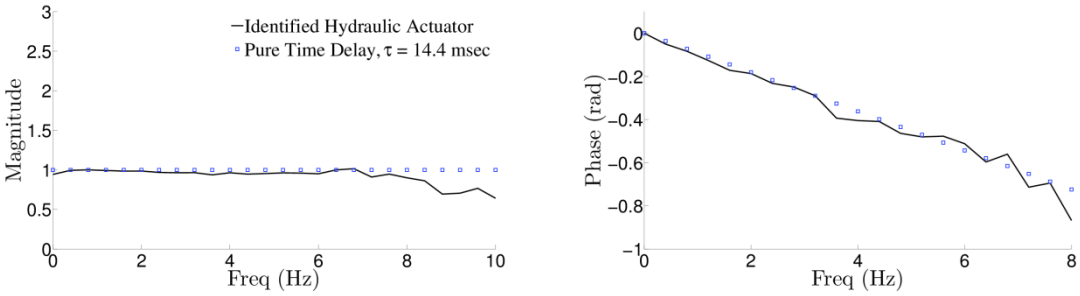

Fig. 16 Frequency responses of the hydraulic actuator and a pure time delay system

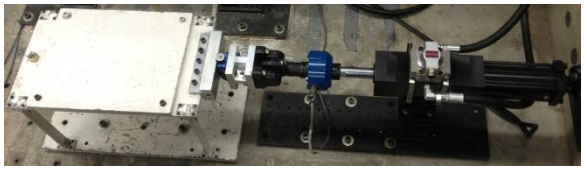

Fig. 17 Physical substructure and transfer system used in this RTHS

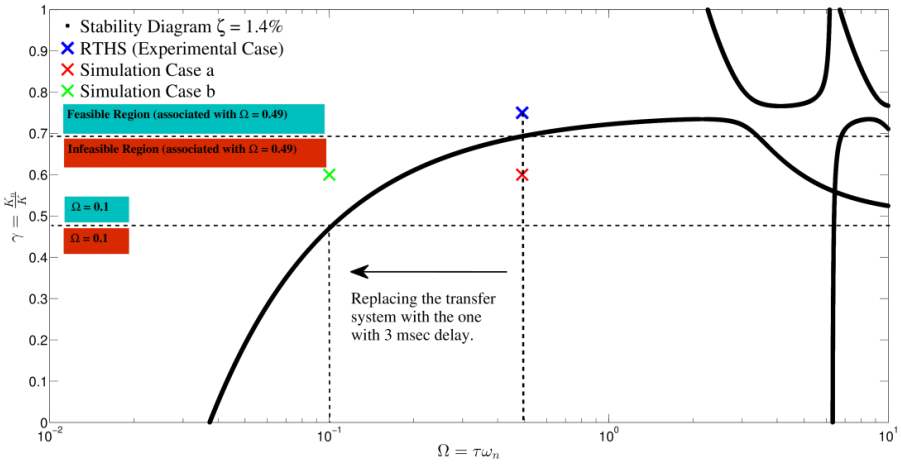

Fig. 18 Location of the RTHS case study and simulation cases on the RTHS stability diagram

As shown in Fig. 18, $\Omega_1 = \tau\omega_n = 0.49$ divides the diagram into two sections, feasible region ($0.69 < \gamma < 1$) and infeasible region ($0 < \gamma < 0.69$), and the RTHS case study in Table 2 lies within the feasible region ($\gamma = 0.75$). Fig. 19 shows the results for RTHS and the reference

structure in the time and frequency domains. Clearly, the RTHS system demonstrated here is stable and the corresponding NRMSE using Eq. (47) is 0.9%.

$$NRMSE\% = \frac{RMS[x_{SIM}(t) - x_{RTHS}(t)]}{max[x_{SIM}(t)] - min[x_{SIM}(t)]} \times 100 \tag{47}$$

Fig. 18 also shows that how a smaller Ω (e.g., $\Omega_2 = 0.1$) yields a wider range of feasible region in this setup ($0.47 < \gamma < 1$).

5.2 Illustrative simulations

Two MATLAB simulations of RTHS are also conducted using the parameters listed in Table 3 subject to the ChiChi earthquake ground acceleration with the peak acceleration of 0.061g, see Fig. 14.

The stability of these two cases can be also identified using the RTHS stability diagram in Fig. 18. The simulation results in Figs. 20(a) and 20(b) show that case a and case b are unstable and stable, respectively. The simulation results are in full agreement with the results from the RTHS stability diagram in Fig. 18 (indicated as simulation case a and simulation case b).

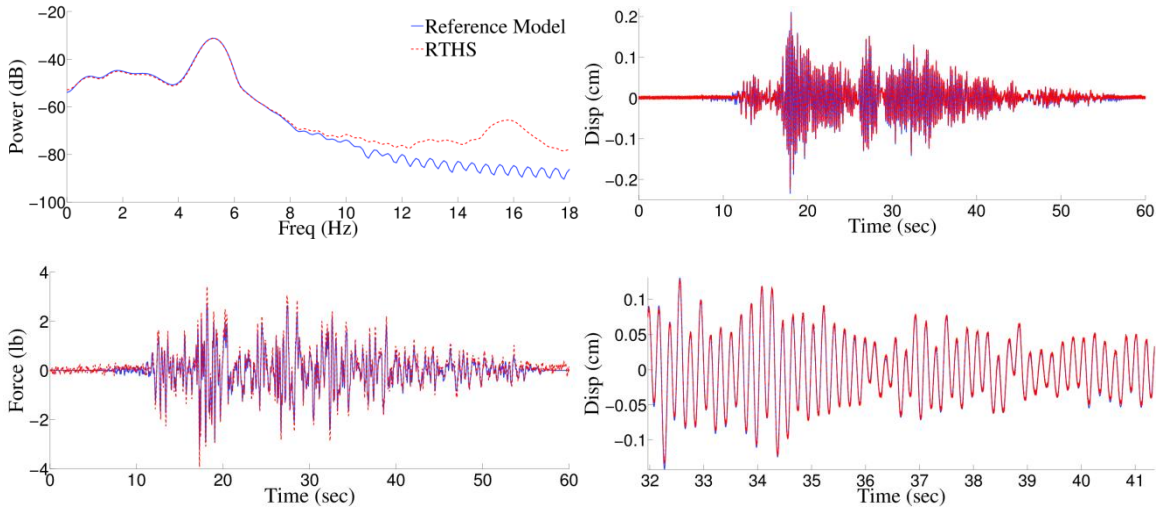

Fig. 19 Responses of RTHS and the reference model, (a) frequency domain, (b) time domain, (c) time domain, (d) time domain (zoomed in)

Table 3 Parameters of the two MATLAB simulations of RTHS

	α	β	γ	ζ	$\omega_n(rad/sec)$	Ω
Case a	0.75	0.82	0.6	0.014	32.9	0.49
Case b	0.75	0.82	0.6	0.014	32.9	0.1

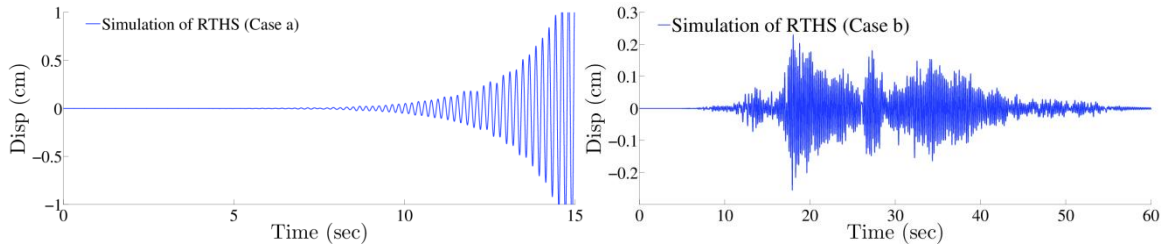

Fig. 20 Responses of simulations of RTHS (case a and case b) subject to ChiChi seismic excitation with PGA = 0.061g

In this work, based on the performance of the transfer system and the existence of various sources of time delay, an RTHS case study and two simulations of RTHS have been conducted. Using the RTHS stability diagram, we have demonstrated: (i) how the stability of a SDOF RTHS is identified, (ii) the most effective ways to stabilize an unstable simulation, and (iii) how the feasible and infeasible regions vary as functions of the performance of the transfer system, computational delay, and communication delay. Moreover, the RTHS stability diagram demonstrates the fact that higher modes of a reference structure are highly sensitive to time delays and require special treatments to conduct a successful RTHS because for a given Ω_{cr} $(= \omega_n \tau_{cr})$, a larger value for ω_n leads to a smaller value for τ_{cr}.

6. Conclusions

To advance the current knowledge of structural behavior subject to extreme dynamic loading and to mitigate existing threats against civil infrastructure, new technologies in experimental evaluation of civil structures must be embraced. RTHS represents an alternative experimental technique to evaluate the performance of rate-dependent behavior in civil structures in the laboratory. To fully leverage the capabilities of RTHS, guidelines are needed to address some key issues associated with its use. In this work, the major issues investigated are the minimum requirements of the transfer system control, the minimum required sampling frequency, the structural characteristics of the reference structure, the most effective changes to stabilize an unstable simulation due to the transfer system limitations, and nonlinearity in the physical substructure. This paper introduced the RTHS stability switch criterion which serves as an experimental design guideline associated with the minimum stability/control requirements to conduct a successful RTHS. In addition, through experimental and numerical simulations, the use of the RTHS stability switch criterion is demonstrated for planning RTHS.

Acknowledgments

This material is based in part upon work supported by the NSF under grant no. NSF-1136075.

References

Ahmadizadeh, M. (2007), *Real-time seismic hybrid simulation procedures for reliable structural performance testing*, University of New York at Buffalo.

Beretta, E. and Kuang, Y. (2002), "Geometric stability switch criteria in delay differential systems with delay dependent parameters", *SIAM J. Math. Anal.* **33**(5), 1144-1165. doi:10.1137/S0036141000376086.

Carrion, J.E. and Spencer Jr., B.F. (2007), M*odel-based strategies for real-time hybrid testing*, Newmark Structural Engineering Laboratory, University of Illinois at Urbana-Champaign.

Castaneda, N., Gao, X. and Dyke, S.J. (2012), "A real-time hybrid testing platform for the evaluation of seismic mitigation in building structures", *Proceedings of the 2012 Structures Congress Conference*.

Chen, C., Ricles, J.M., Karavasilis, T.L., Chae, Y. and Sause, R. (2012), "Evaluation of a real-time hybrid simulation system for performance evaluation of structures with rate dependent devices subjected to seismic loading", *Eng. Struct*., **35**, 71-82. doi:10.1016/j.engstruct.2011.10.006.

Chen, C. and Ricles, J.M. (2009), "Analysis of actuator delay compensation methods for real-time testing", *Eng. Struct*., **31**(11), 2643-2655. doi:10.1016/j.engstruct.2009.06.012.

Chen, C., Valdovinos, J. and Santiallno, H. (2013), "Reliability assessment of real-time hybrid simulation results for seismic hazard mitigation", *Proceedings of the Structures Congress 2013*, 2346-2357. Reston, VA: American Society of Civil Engineers. doi:10.1061/9780784412848.205.

Christenson, R., Lin, Y.Z., Emmons, A. and Bass, B. (2008). "Large-scale experimental verification of semiactive control through real-time hybrid simulation1", *J. Struct. Eng.- ASCE* **134**(4), 522-534. doi:10.1061/(ASCE)0733-9445(2008)134:4(522).

Darby, A.P., Williams, M.S. and Blakeborough, A. (2002), "Stability and delay compensation for real-time substructure testing", *J. Eng. Mech. - ASCE* **128**(12), 1276-1284. doi:10.1061/(ASCE)0733-9399(2002) 128:12(1276).

Dihoru, L, and Bonzi, A. (2010), *Performance requirements of actuation systems for shaking table and pseudo-dynamic testing*, *D*eliverable D12.1, SERIES: Seismic Engineering Research Infrastructures for European Synergies.

Dyke, S.J., Stojadinovic, B., Arduino, P., Garlock, M., Luco, N., Ramirez, J.A. and Yim, S. (2010), "2020 vision for earthquake engineering research: report on an open space technology workshop on the future of earthquake engineering", Vol. 20. http://nees.org/resources/1636.

Dyke, S.J., Spencer Jr., B.F., Quast, P. and Sain, M.K. (1995), "Role of control-structure interaction in protective system design", *J. Eng. Mech.- ASCE*, 121(2), 322-338. doi:10.1061/(ASCE)0733-9399(1995) 121:2(322).

Friedman, A.J., Zhang, J., Phillips, B., Jiang, Z., Agrawal, A., Dyke, S.J., Ricles, J., Spencer Jr., B.F., Sause, R. and Christenson, R. (2010), "Accommodating MR damper dynamics for control of large scale structural systems", *Proceedings of the 5th World Conference on Structural Control and Monitoring*, Tokyo, Japan. https://nees.org/resources/674.

Gao, X. (2012), "Development of a robust framework for real-time hybrid simulation: from dynamical system, motion control to experimental error verification", NEES. http://nees.org/resources/5065.

Horiuchi, T., Inoue, M., Konno, T. and Yamagishi, W. (1999), "Development of a real-time hybrid experimental system using a shaking table (Proposal of Experimental Concept and Feasibility Study with Rigid Secondary System)", *JSME Int.*, **42**(2), 255-264.

Horiuchi, T., Nakagawa, M. Sugano, M. and Konno, T. (1996), "Development of a real-time hybrid experimental system with actuator delay compensation", *Proceedings of the 11th World Conf. Earthquake Engineering*.

Jiang, Z. and Christenson, R. (2011), "A comparison of 200 kN magneto-rheological damper models for use in real-time hybrid simulation pre-testing", *Smart Mater. Struct*., **20**(6), 065011. doi:10.1088/0964-1726/20 /6/065011.

MacDonald, N. (1989), *Biological Delay Systems: Linear Stability Theory*, Cambridge: Cambridge University Press.

Maghareh, A. and Dyke, S.J. (2013), "Stability and performance analysis of SDOF real-time hybrid simulation", https://engineering.purdue.edu/IISL/publicationtr.html.

Maghareh, A., Dyke, S.J., Ou, G. and Qian, Y. (2013), "Investigation of uncertainties associated with actuation modeling error and sensor noise on real-time hybrid simulation performance", *Proceedings of the 2013 International Conference on Computing, Networking and Communications (ICNC)*, 210-214. IEEE. doi:10.1109/ICCNC.2013.6504082. http://ieeexplore.ieee.org/lpdocs/epic03/wrapper.htm?arnumber=6504082.

Maghareh, A., Dyke, S.J., Prakash, A. and Bunting. G.B. (2013), "Establishing a predictive performance indicator for real-time hybrid simulation", *Earthq. Eng. Struct. D.*, (in press).

Maghareh, A., Dyke, S.J., Prakash, A., Bunting, G. and Lindsay, P. (2012), "Evaluating modeling choices in the implementation of real-time hybrid simulation", *Proceedings of the EMI/PMC 2012 Joint Conference of the Engineering Mechanics Institute and the 11th ASCE Joint Specialty Conference on Probabilistic Mechanics and Structural Reliability*. Notre Dame, IN. https://nees.org/resources/4699.

Maghareh, A., Lin, F., Dyke, S.J. and Prakash, A. (2014), "Development of new predictive stability and performance metrics for real-time hybrid simulation", NEES, doi:TBD. https://nees.org/warehouse/project/1205/.

Maghareh, A., Dyke, S.J., Prakash, A., Bunting, G. and Lindsay, P. (2012), "Evaluating modeling choices in the implementation of real-time hybrid simulation", *Proceedings of the 11th ASCE Joint Specialty Conference on Probabilistic Mechanics and Structural Reliability*.

Mosqueda, G., Stojadinovic, B. and Mahin, S. (2005), "Implementation and accuracy of continuous hybrid simulation with geographically distributed substructures", http://research.eerc.berkeley.edu/nees/Events/200604a--workshop-hybridsim/ ERCreport-Hybrid02.pdf.

Mosqueda, G., Stojadinovic, B. and Mahin, S. (2007), "Real-time error monitoring for hybrid simulation. part II: structural response modification due to errors", *J. Struct. Eng. - ASCE*, **133**(8), 1109-1117. doi:10.1061/(ASCE)0733-9445(2007)133:8(1109).

Mosqueda, G., Stojadinovic, B. and Mahin, S.A. (2007a), "Real-time error monitoring for hybrid simulation. part I: methodology and experimental verification", *J. Struct. Eng. - ASCE*, **133**(8), 1100-1108. doi:10.1061/(ASCE)0733-9445(2007)133:8(1100). http://ascelibrary.org/doi/abs/10.1061/(ASCE)0733-9445(2007)133:8(1100).

Mosqueda, G., Stojadinovic, B. and Mahin, S.A. (2007b), "Real-time error monitoring for hybrid simulation. part II: structural response modification due to errors", *J. Struct. Eng.- ASCE*, **133**(8) 1109-1117. doi:10.1061/(ASCE)0733-9445(2007)133:8(1109). http://ascelibrary.org/doi/abs/10.1061/(ASCE)0733-9445(2007)133:8(1109).

Ou, G., Dyke, S.J., Wu, B., Ozdagli, A.I. and Li, B. (2013), "Robusted integrated actuator control strategy for real time hybrid simulation", *Proceedings of the SERIES Concluding Workshop - Joint with US-NEES "Earthquake Engineering Research Infrastructures"*, Ispra.

Phillips, B.M. and Spencer Jr., B.F. (2013), "Model-based multiactuator control for real-time hybrid simulation", *J. Eng. Mech.- ASCE*, **139**(2), 219-228. doi:10.1061/(ASCE)EM.1943-7889.0000493.

Schellenberg, A. and Mahin, S. (2006), "Integration of hybrid simulation within the general-purpose computational framework opensees", *Proceedings of the 100th Anniversary Earthquake Conference*.

Shao, X., Reinhorn, A.M. and Sivaselvan, M.V. (2011), "Real-time hybrid simulation using shake tables and dynamic actuators", *J. Struct. Eng. - ASCE*, **137**(7), 748-760. doi:10.1061/(ASCE)ST.1943-541X.0000314.

Shing, P.B., Wei, Z., Jung, R.Y. and Stauffer, E. (2004), "NEES fast hybrid test system at the university of Colorado", *Proceedings of the 13th World Conference on Earthquake Engineering* (3497).

Shing, P.B. and Mahin, S.A. (1984), "Pseudodynamic test method for seismic performance evaluation: theory and implementation".

Shing, P.B., Nakashima, M. and Bursi, O.S. (1996), "Application of psuedodynamic test method to structural research", *Earthq. Spectra*, **12**(1), 29-56.

Wagg, D.J. and Stoten, D.P. (2001), "Substructuring of dynamical systems via the adaptive minimal control synthesis algorithm", *Earthq. Eng. Struct. D.*, **30**(6), 865-877. doi:10.1002/eqe.44.

Wallace, M.I., Sieber, J., Neild, S.A., Wagg, D. J. and Krauskopf, B. (2005), "Stability analysis of real-time dynamic substructuring using delay differential equation models", *Earthq. Eng. Struct. D.*, 34(15) 1817-1832. doi:10.1002/eqe.513.

Zhao, J., French, C., Shield, C. and Posbergh, T. (2003), "Considerations for the development of real-time dynamic testing using servo-hydraulic actuation", *Earthq. Eng. Struct. D.*, 32(11), 1773-1794. doi:10.1002/eqe.301.